Slabs, plumes and their interaction: new insights from global anisotropy tomography

Ana M G Ferreira
Seismological Laboratory, Department of Earth Sciences
University College London, UK

Sung-Joon Chang, Manuele Faccenda
Jeroen Ritsema, Hendrik J. van Heijst, John H. Woodhouse, Karin Visser, Jeannot Trampert

UCL Seismolab

Global seismic tomography

S-wave velocity:

- Well-known and reproducible large scale features

Go further:

- Anisotropy, attenuation, … ⇒ Larger discrepancies

Anisotropy:

- Potential indicator of mantle flow
  - Radial anisotropy: PREM

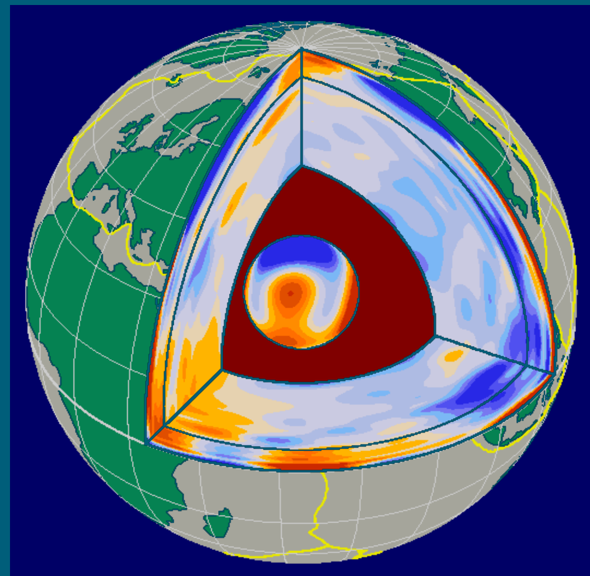

S20RTS Ritsema et al., 1999

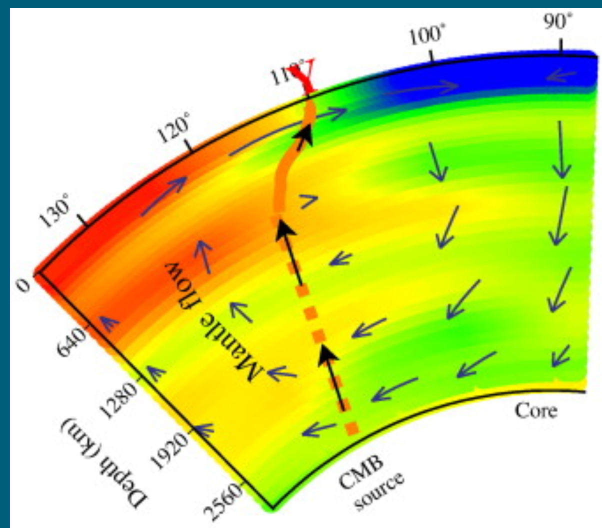

Global seismic tomography – massive data set

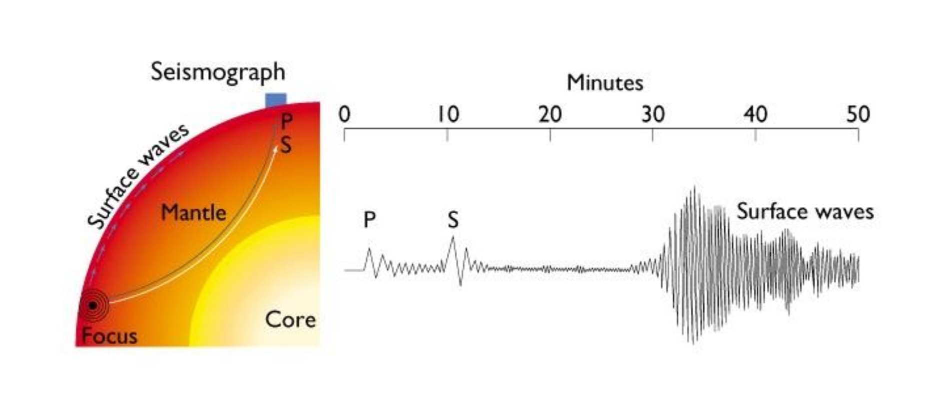

Global seismic tomography – massive data set

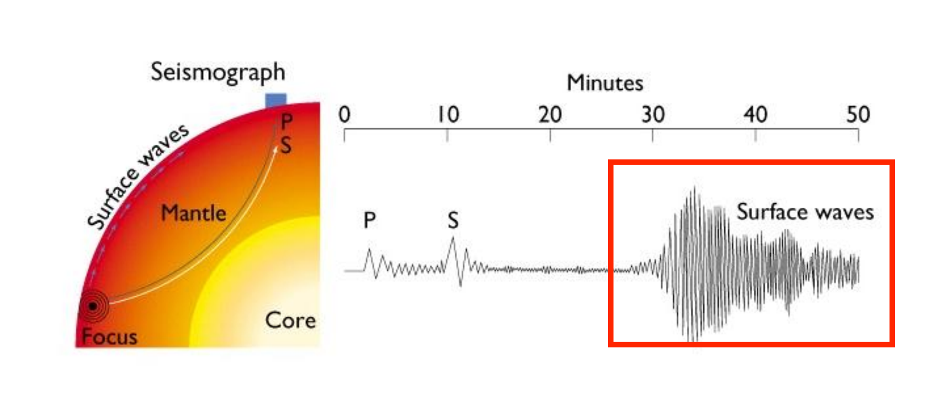

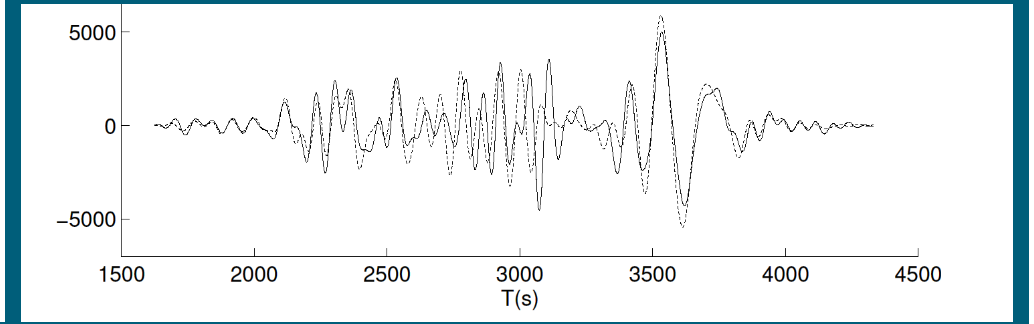

- Over 43,000,000 surface wave phase measurements, T~25-375 s (van Heijst & Woodhouse, 1997; Ritsema et al., 2011; Ekstrom et al. 1997, 2011; Visser et al. 2007) and group velocity data, T~16-150 s (Ritzwoller & Levshin, 1998)

Global seismic tomography – massive data set

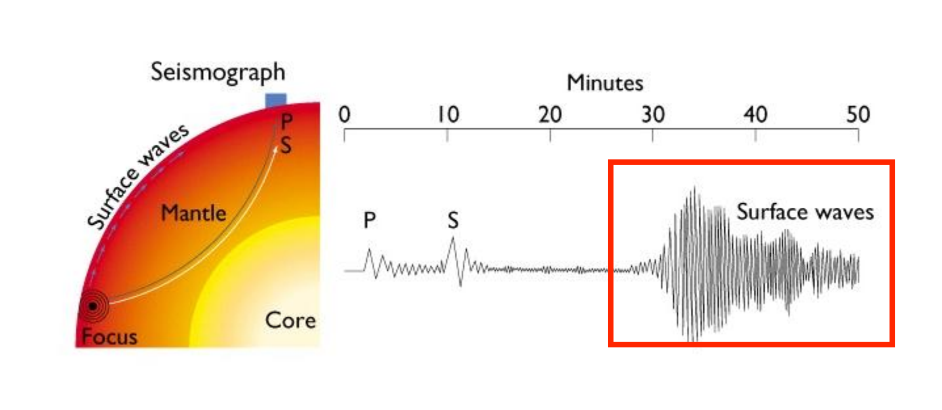

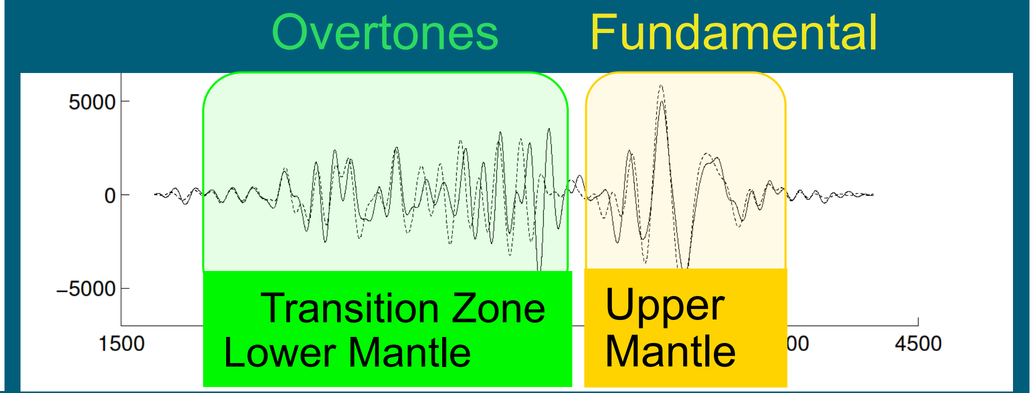

- Over 43,000,000 surface wave phase measurements, T~25-375 s (van Heijst & Woodhouse, 1997; Ritsema et al., 2011; Ekstrom et al. 1997, 2011; Visser et al. 2007) and group velocity data, T~16-150 s (Ritzwoller & Levshin, 1998)

- Fundamental and higher mode Rayleigh (up to the 6th overtone) and Love (up to the 5th overtone) waves

Global seismic tomography – massive data set

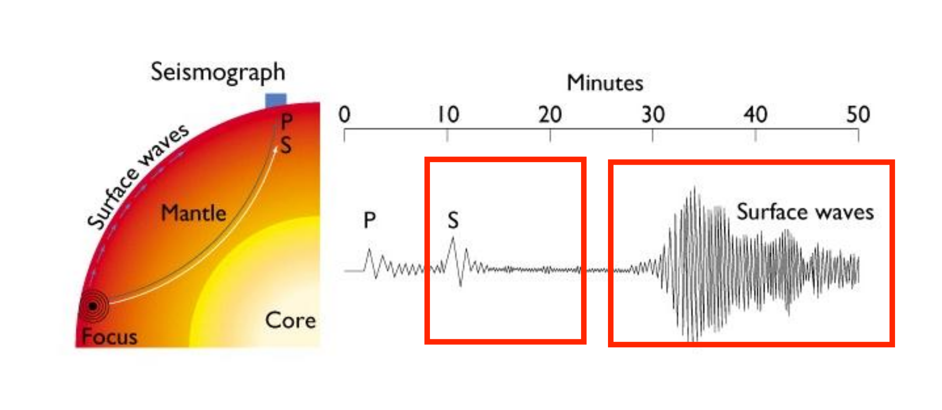

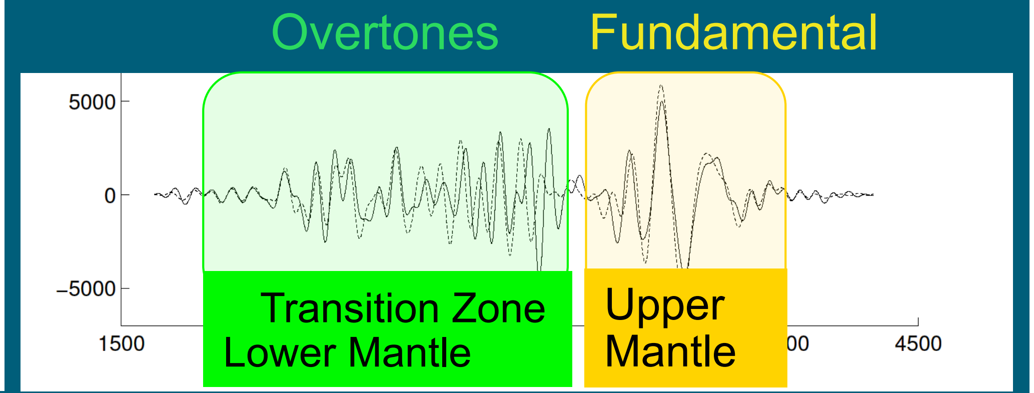

- Over 43,000,000 surface wave phase measurements, T~25-375 s (van Heijst & Woodhouse, 1997; Ritsema et al., 2011; Ekstrom et al. 1997, 2011; Visser et al. 2007) and group velocity data, T~16-150 s (Ritzwoller & Levshin, 1998)

- Fundamental and higher mode Rayleigh (up to the 6th overtone) and Love (up to the 5th overtone) waves

- Teleseismic travel-times: S, SS, SSS, ScS, ScS2, ScS3, SKS, SKKS, depth phases (Ritsema et al., 2011)

Global seismic tomography – massive data set

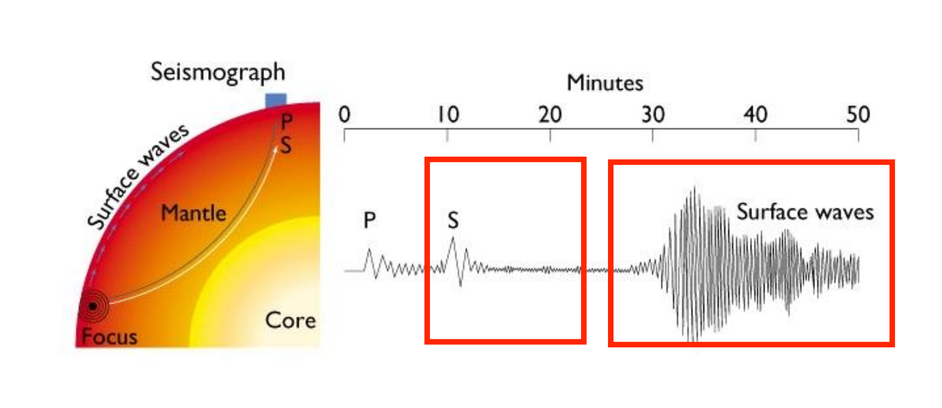

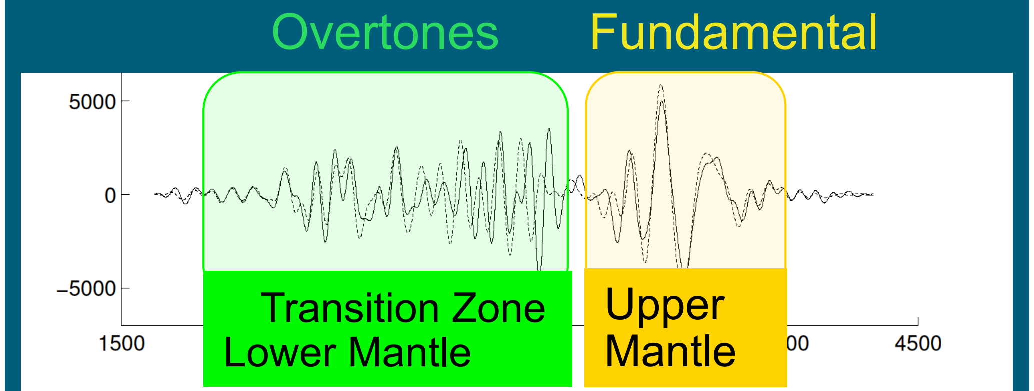

- Over 43,000,000 surface wave phase measurements, T~25-375 s (van Heijst & Woodhouse, 1997; Ritsema et al., 2011; Ekstrom et al. 1997, 2011; Visser et al. 2007) and group velocity data, T~16-150 s (Ritzwoller & Levshin, 1998)

- Fundamental and higher mode Rayleigh (up to the 6th overtone) and Love (up to the 5th overtone) waves

- Teleseismic travel-times: S, SS, SSS, ScS, ScS2, ScS3, SKS, SKKS, depth phases (Ritsema et al., 2011)

Complete and diverse dataset: from the crust to the lowermost mantle

Global seismic tomography – modelling approach

✦ **Model parameters:**

$$v_S^2 = \frac{1}{2}(v_{SV}^2 + V_{SH}^2) \quad + \quad \zeta_S = \frac{V_{SH}^2 - v_{SV}^2}{2v_S^2}$$

+ crustal thickness

✦ 1-D reference model: PREM (itself anisotropic)

✦ **Spatial parameterisation:** 21 spline functions (radially): ~60-300 km; Spherical harmonics up to degree 35 (laterally): ~1,200 km

↓

54,432 parameters

✦ **Forward and inverse modelling:** Great-circle approximation **+** least-squares optimization

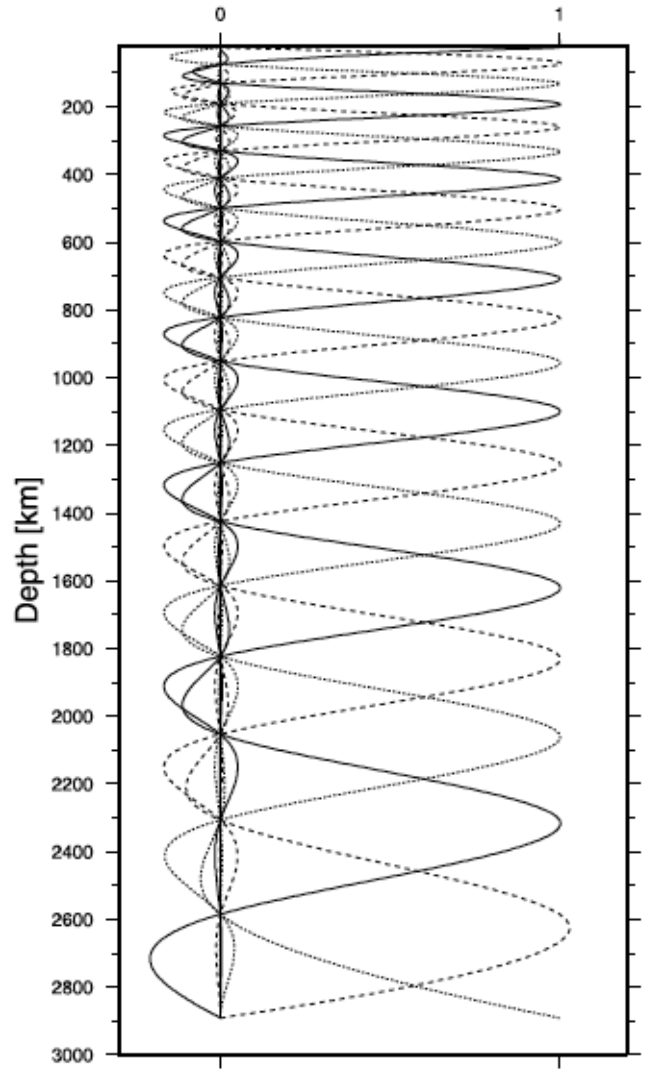

Ferreira et al., JGR, 2010
Chang et al., JGR, 2015
Chang & Ferreira, BSSA, 2016

Global seismic tomography – modelling approach

- **Model parameters:**

$$v_S^2 = \frac{1}{2}(v_{SV}^2 + V_{SH}^2) \quad + \quad \zeta_S = \frac{V_{SH}^2 - v_{SV}^2}{2v_S^2}$$

+ crustal thickness

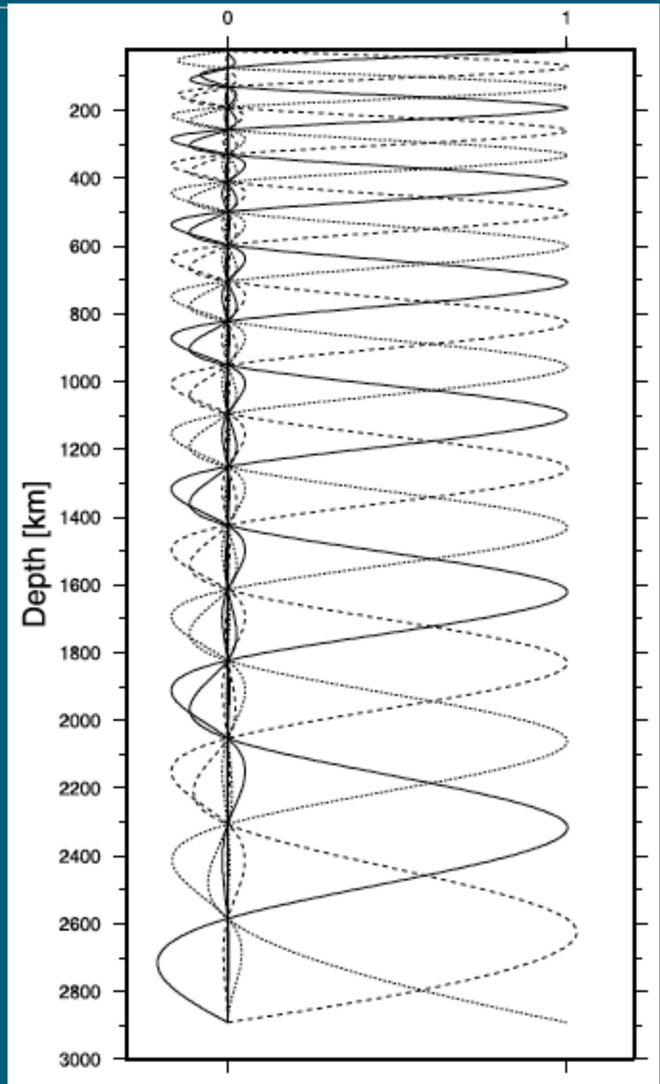

- 1-D reference model: PREM (itself anisotropic)

- **Spatial parameterisation:** 21 spline functions (radially): ~60-300 km; Spherical harmonics up to degree 35 (laterally): ~1,200 km

↓

54,432 parameters

- **Forward and inverse modelling:** Great-circle approximation + least-squares optimization

GCA ✔

OK for phase data for current global models (Parisi & Ferreira,GJI, 2016)

Isotropic S-velocity

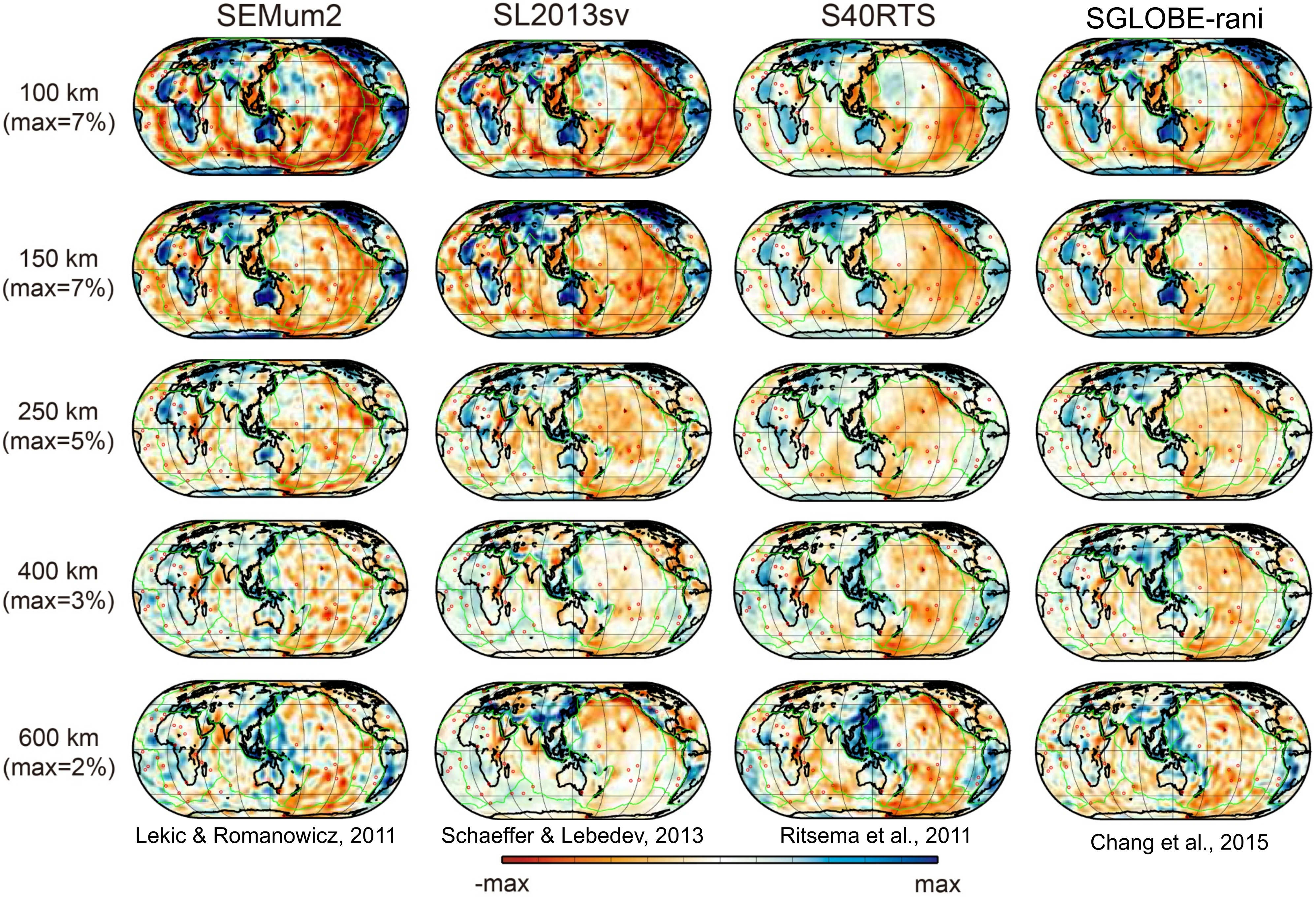

Isotropic S-velocity

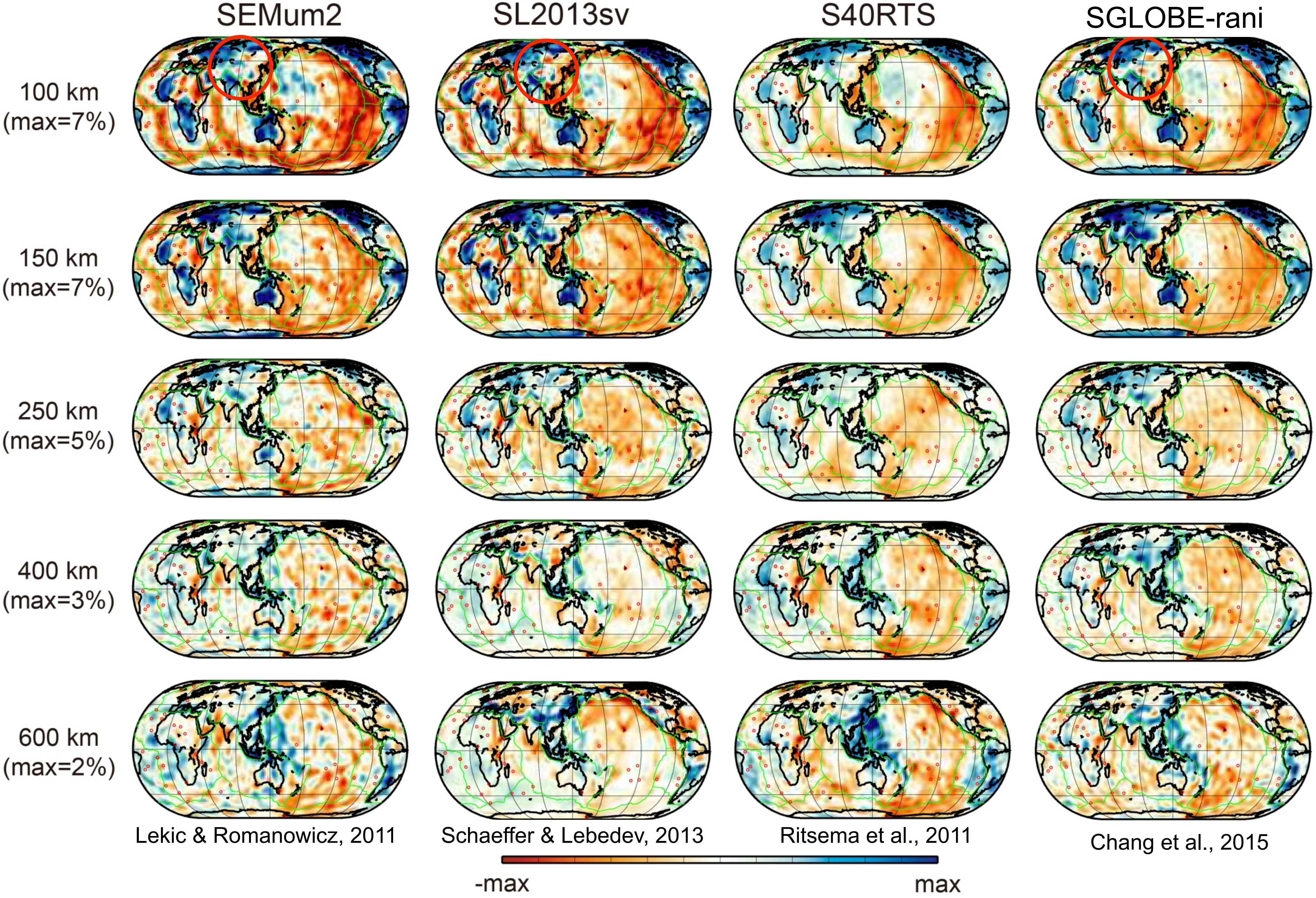

Isotropic S-velocity

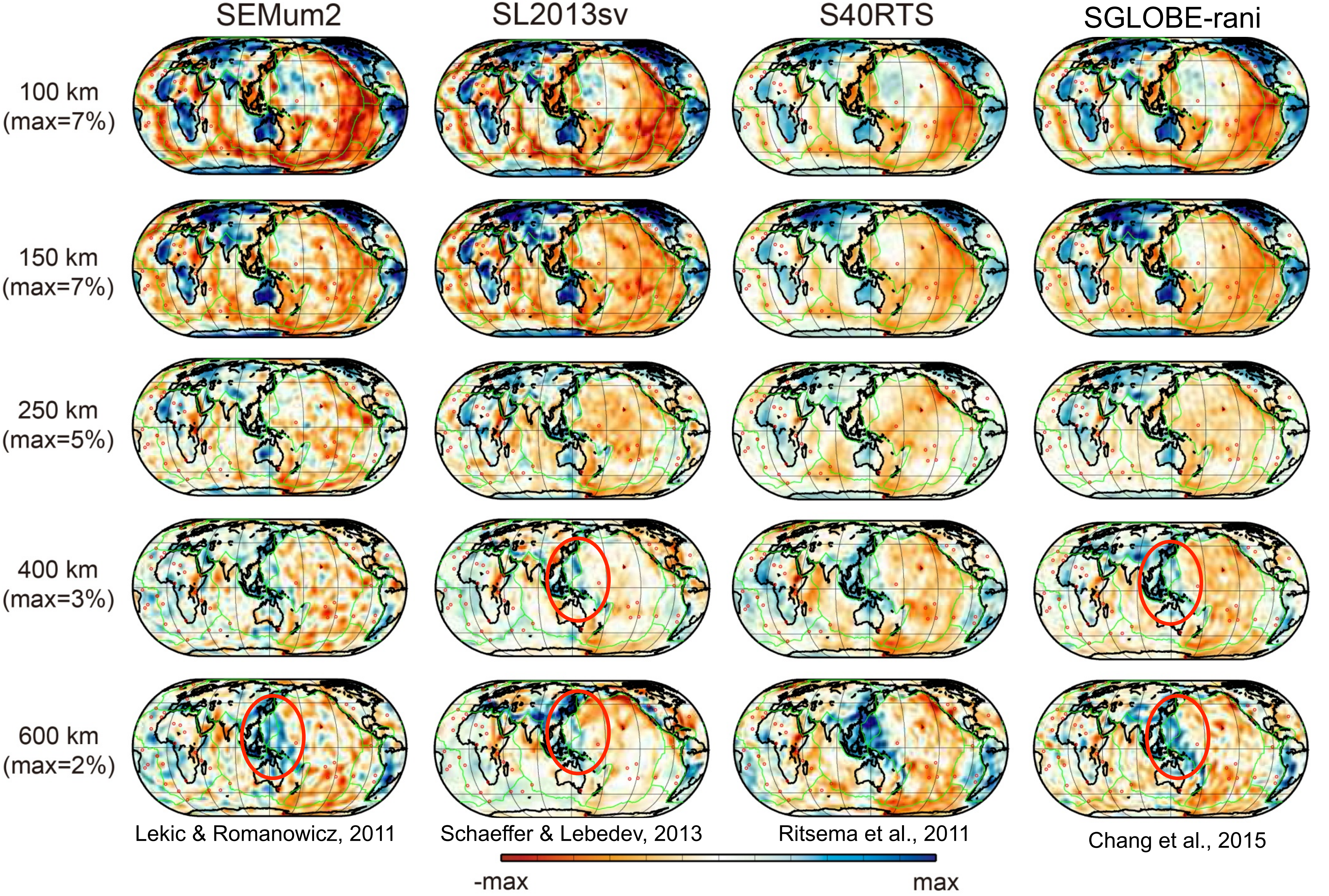

Radial anisotropy $\frac{d\xi}{\xi}$ $\xi = V_{SH}^2 / V_{SV}^2$

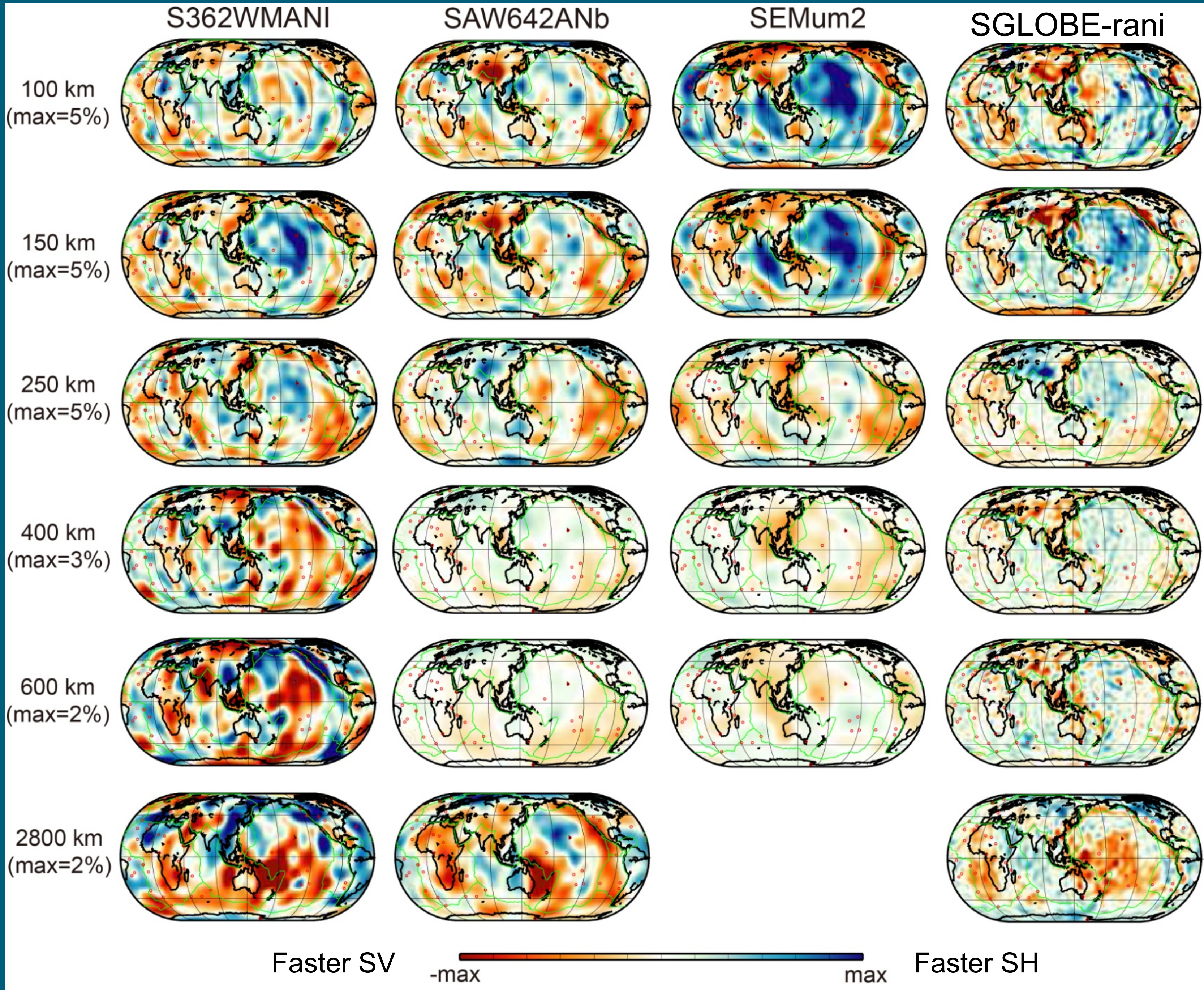

Radial anisotropy $\frac{d\xi}{\xi}$

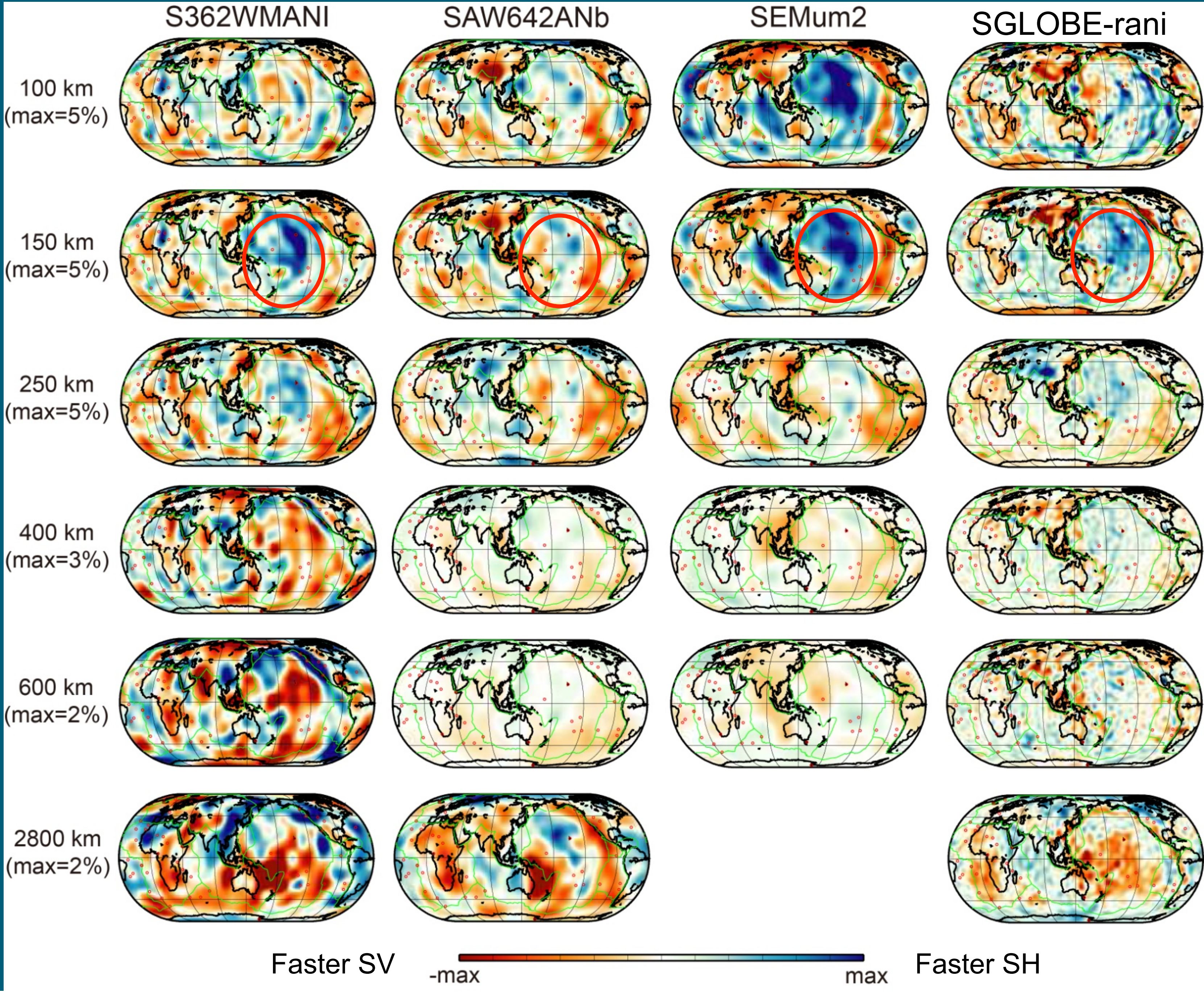

Radial anisotropy $\frac{d\xi}{\xi}$

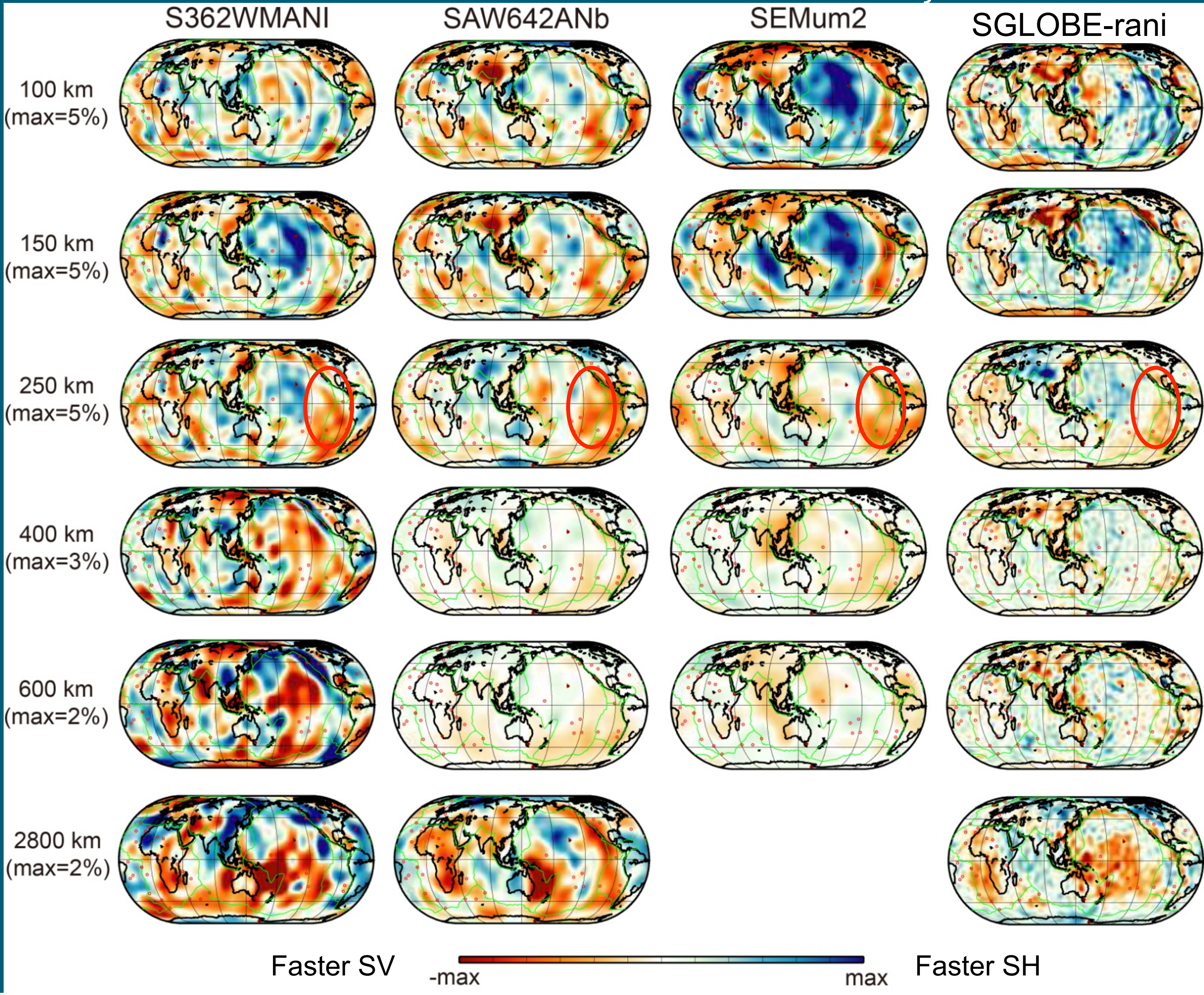

Radial anisotropy $\frac{d\xi}{\xi}$

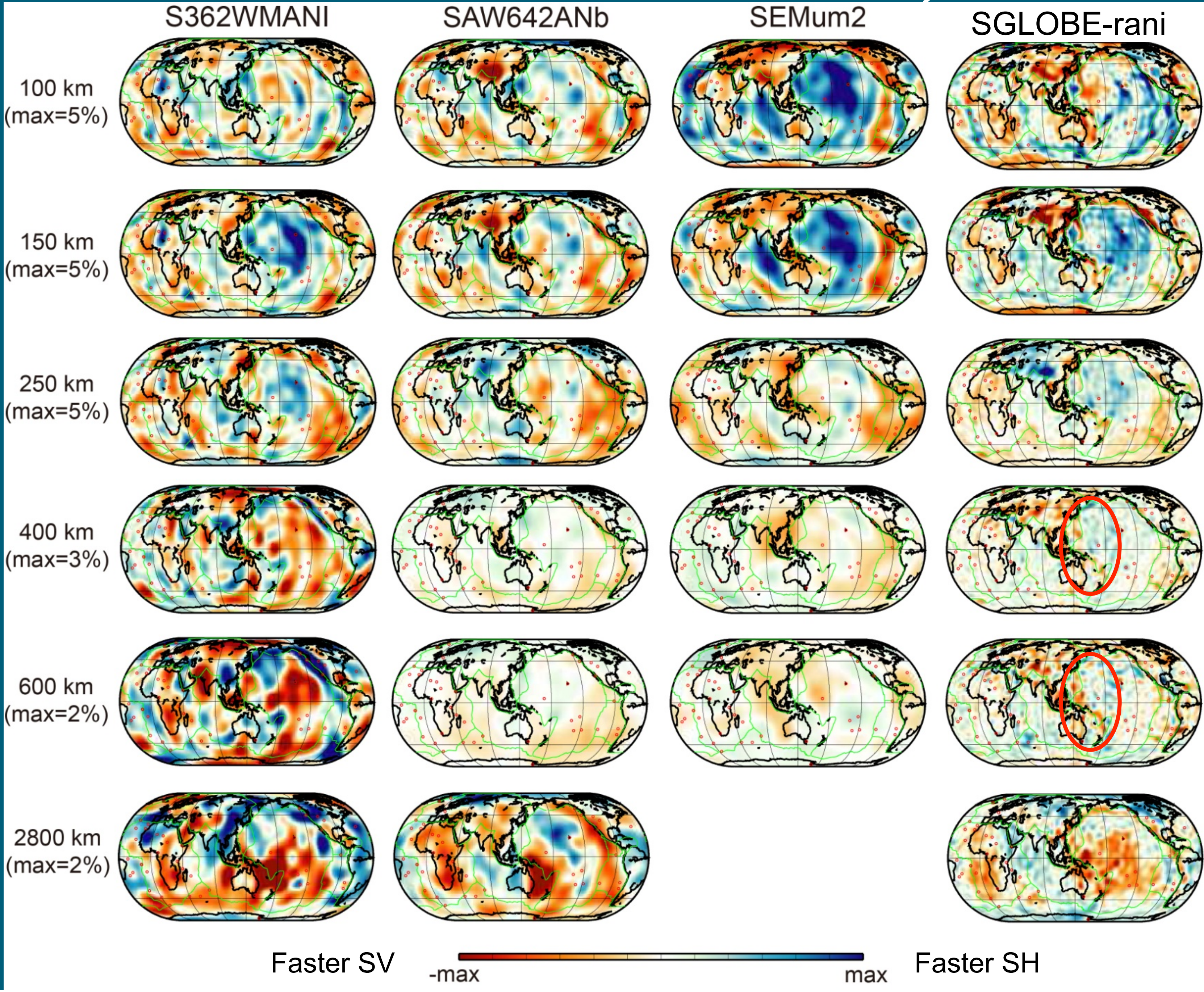

Radial anisotropy $\frac{d\xi}{\xi}$

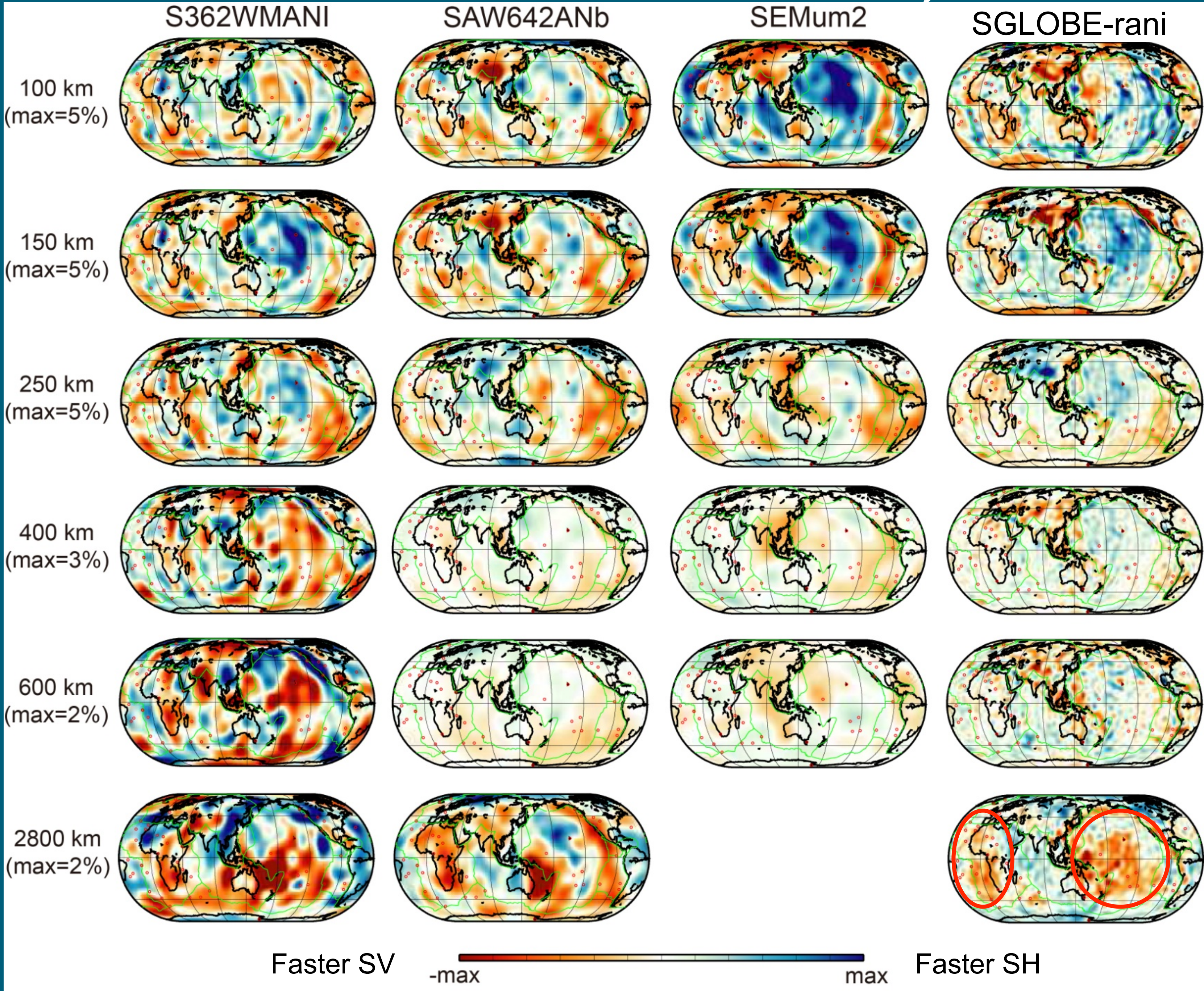

Robustness tests

Input model

Output model

Isotropic structure

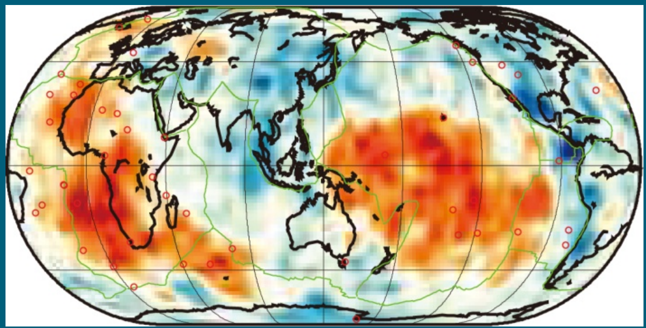

Anisotropic structure

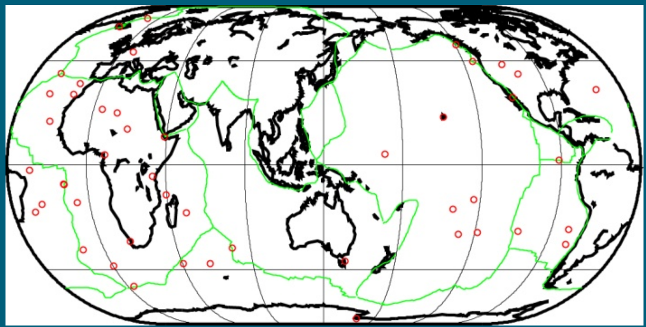

2800 km

Chang et al., Tectonophys., 2014

Robustness tests

Input model

Output model

Isotropic structure

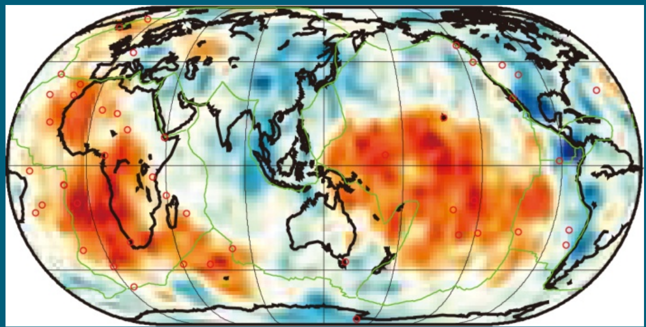

Isotropic structure

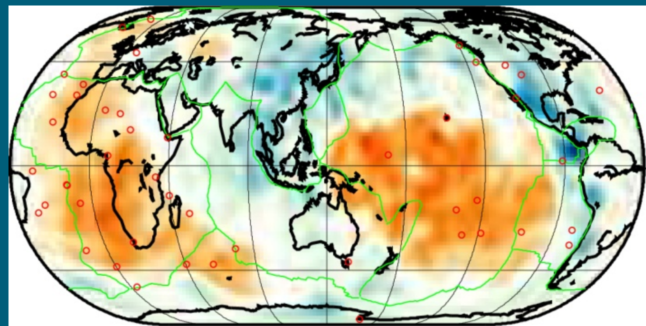

Anisotropic structure

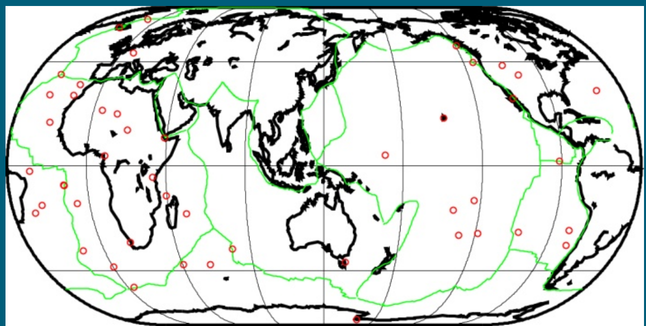

Anisotropic structure

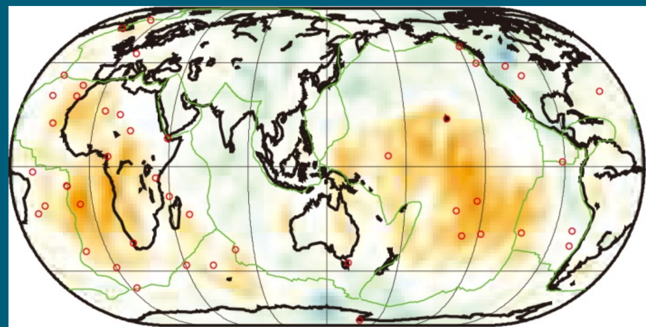

2800 km

Chang et al., Tectonophys., 2014

Robustness tests

Input model

Isotropic structure

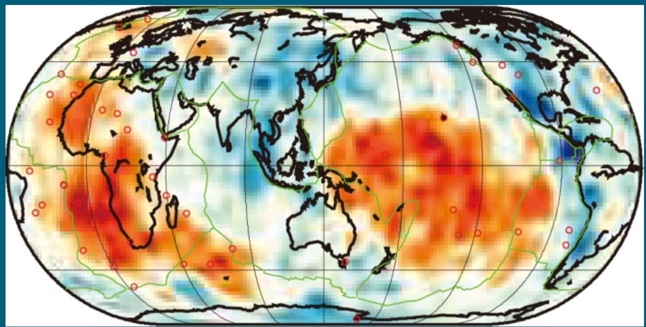

Output model

Anisotropic structure

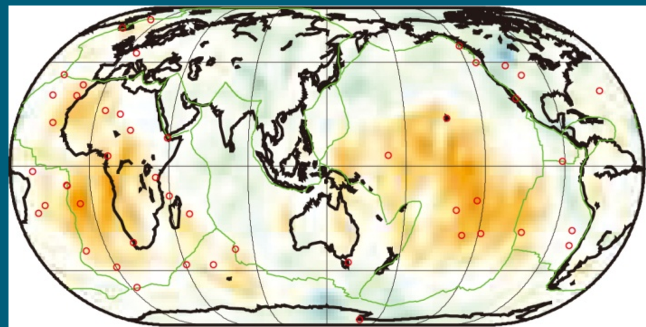

2800 km

Chang et al., Tectonophys., 2014

Robustness tests

Input model

Isotropic structure

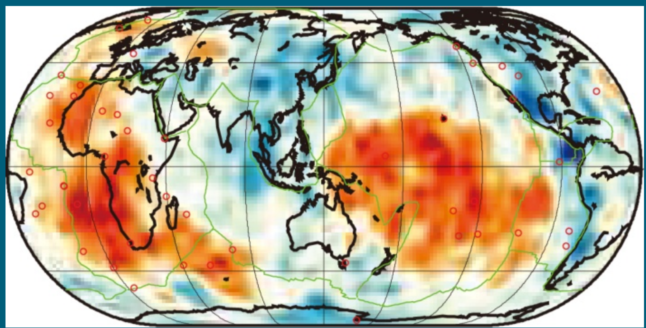

Output model

Anisotropic structure

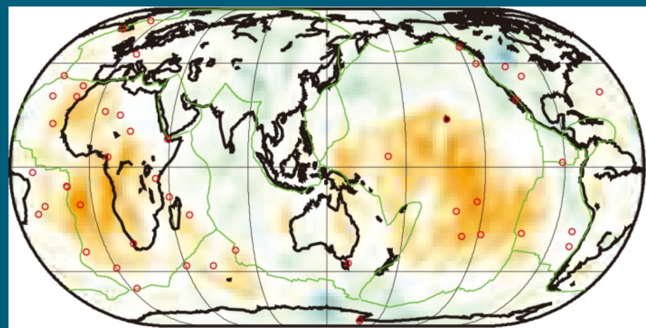

Anisotropic model from real data inversion

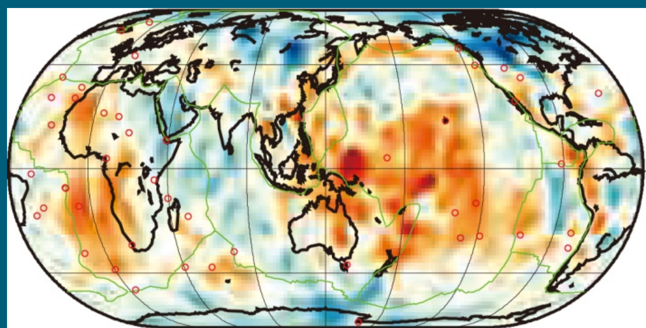

2800 km

Chang et al., Tectonophys., 2014

Global radial anisotropy: transition zone

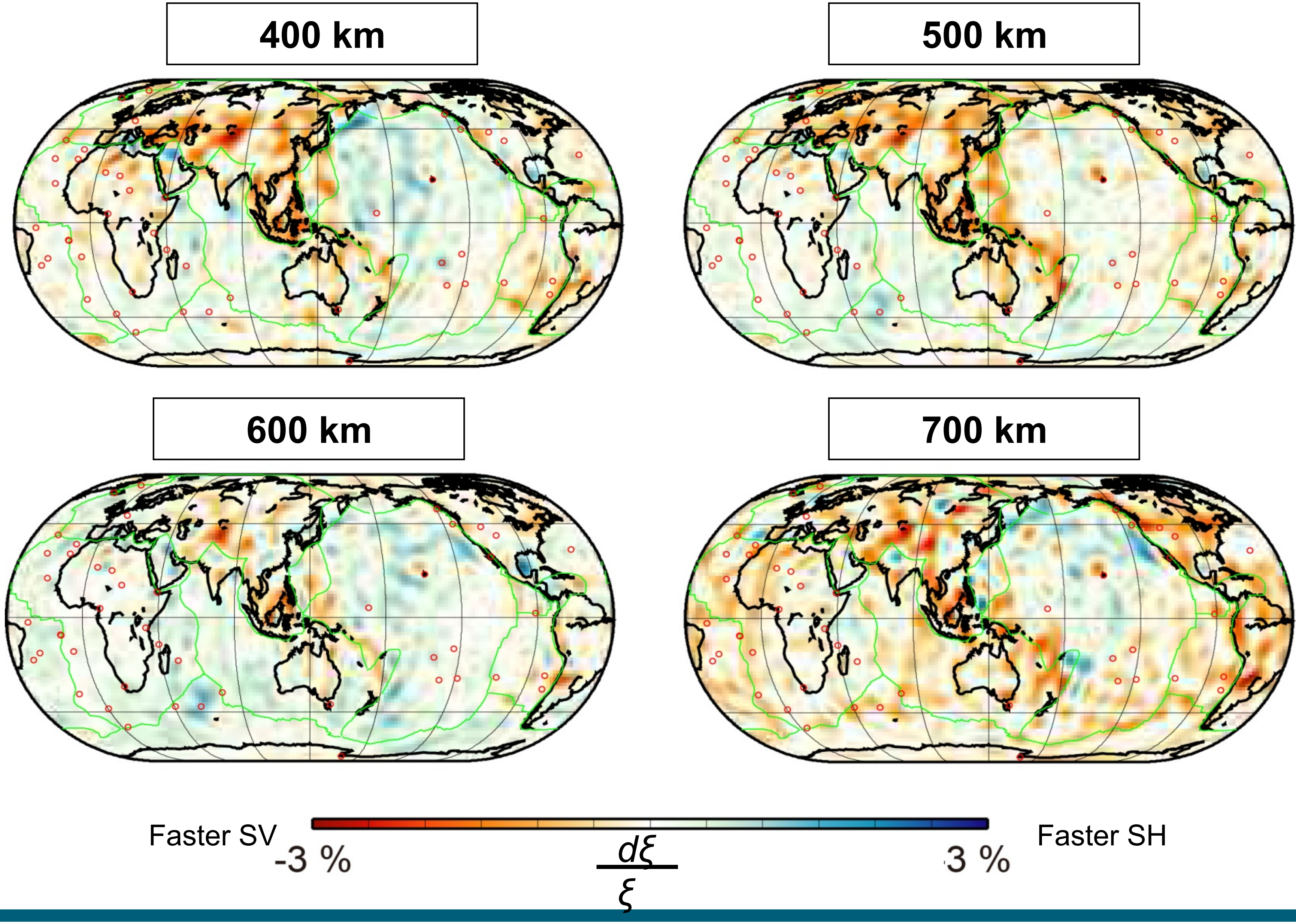

Radial anisotropy:
Subduction zones

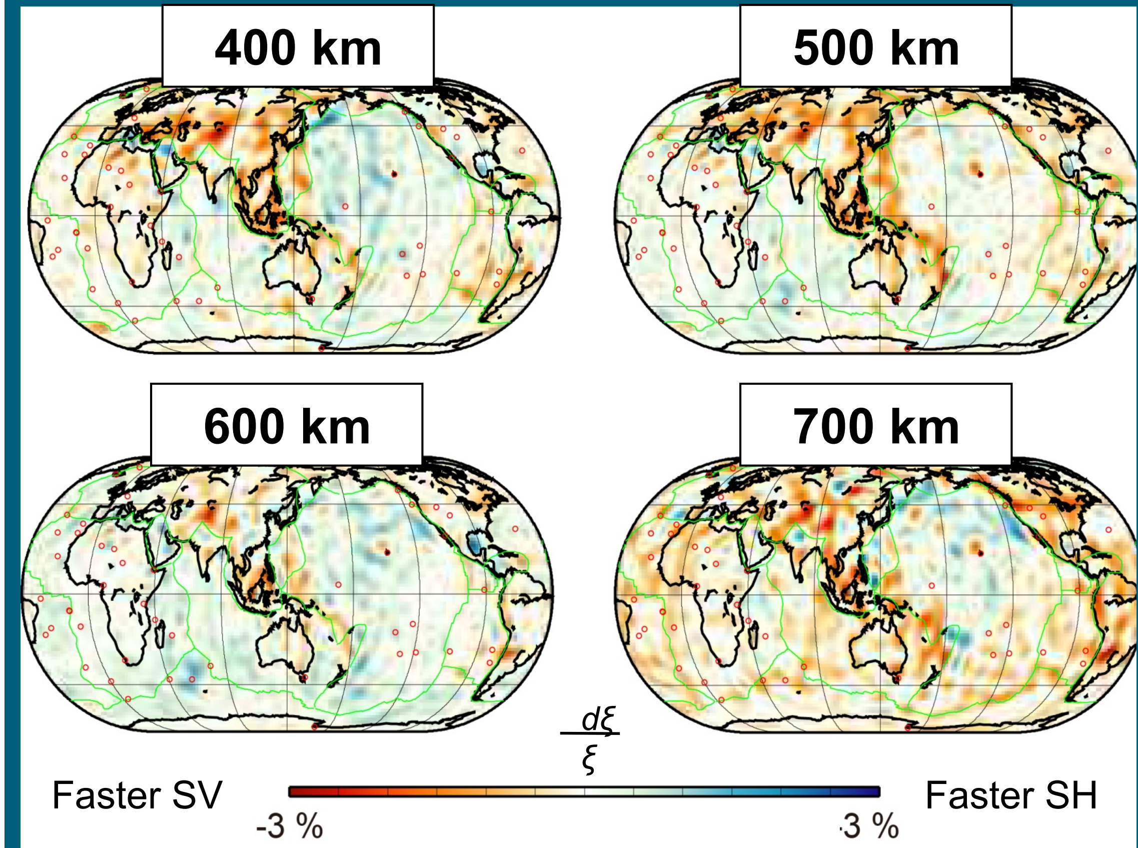

- **SPO** due to laminated structures within stagnant slabs?

Radial anisotropy: Subduction zones

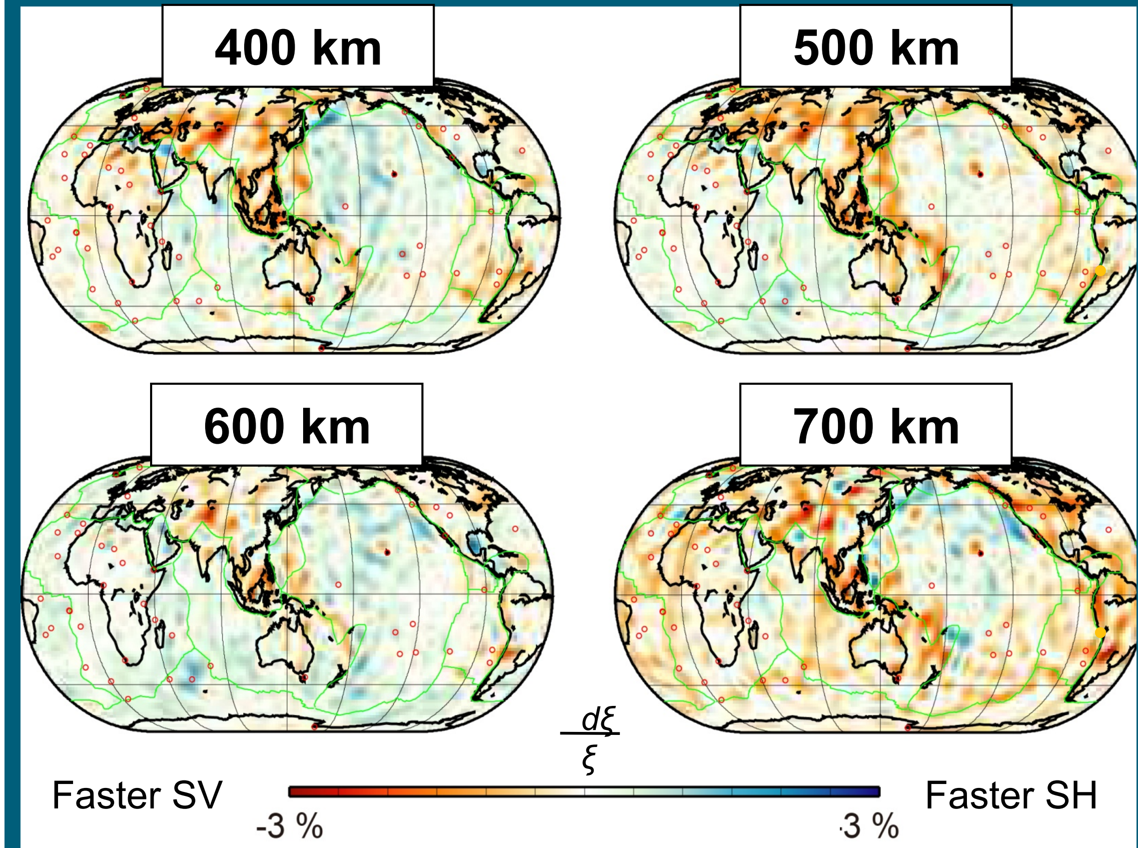

• **SPO** due to laminated structures within stagnant slabs?

- **Wadsleyite (410~520 km)**
  - Kawazoe et al. (2013) – dominant slip direction [001](010) for water content of 50-230 wt. ppm H_2O.
  - Horizontal flow causes faster SV velocity.
- **Ringwoodite (520~660 km)**
  - Weakly anisotropic (Mainprice et al., 2007)
  - SPO may be responsible for anisotropy observed at this depth.
- **Bridgmanite (> 660 km)**
  - Anisotropic in uppermost lower mantle conditions (e.g., Cordier et al., 2004; Mainprice et al., 2008; Tsujino et al., 2016)

+ hydrous phases, ….

Radial anisotropy: Subduction zones

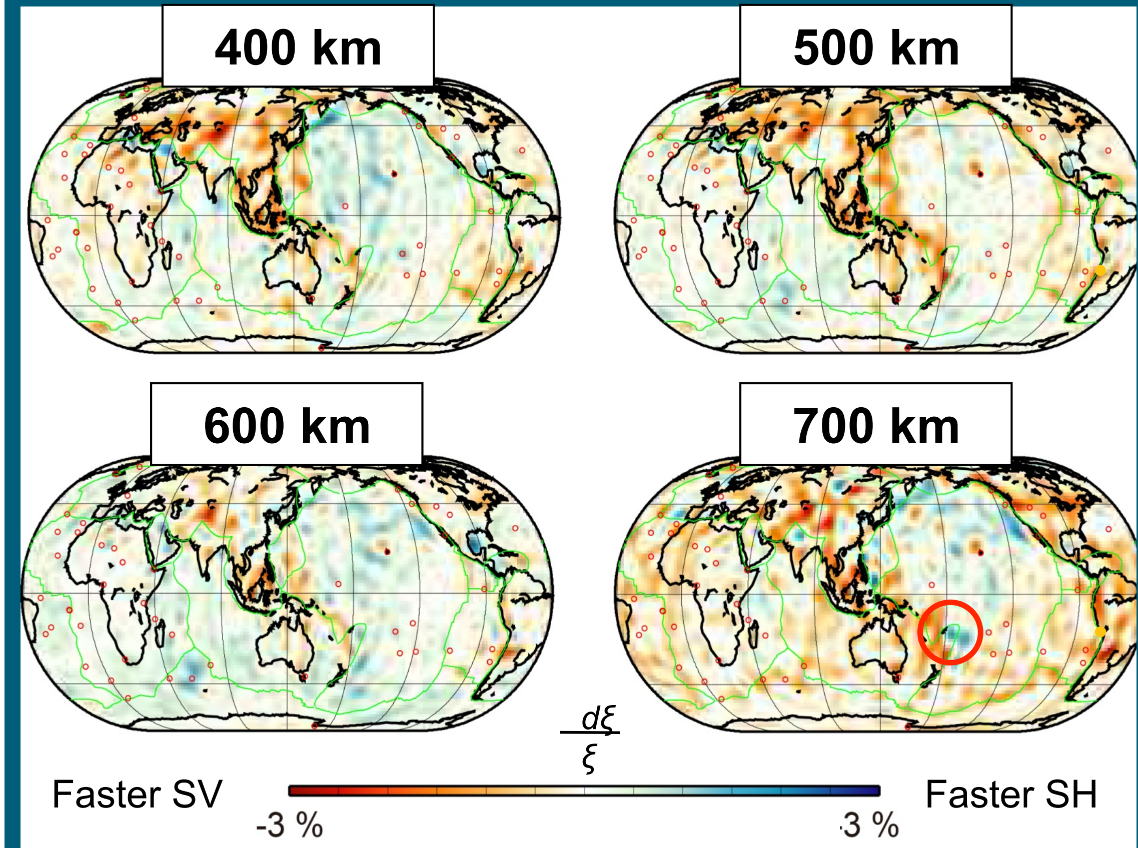

• **SPO** due to laminated structures within stagnant slabs?

- **Wadsleyite (410~520 km)**
  – Kawazoe et al. (2013) – dominant slip direction [001](010) for water content of 50-230 wt. ppm H_2O.
  – Horizontal flow causes faster SV velocity.
- **Ringwoodite (520~660 km)**
  – Weakly anisotropic (Mainprice et al., 2007)
  – SPO may be responsible for anisotropy observed at this depth.
- **Bridgmanite (> 660 km)**
  – Anisotropic in uppermost lower mantle conditions (e.g., Cordier et al., 2004; Mainprice et al., 2008; Tsujino et al., 2016)

+ hydrous phases, ….

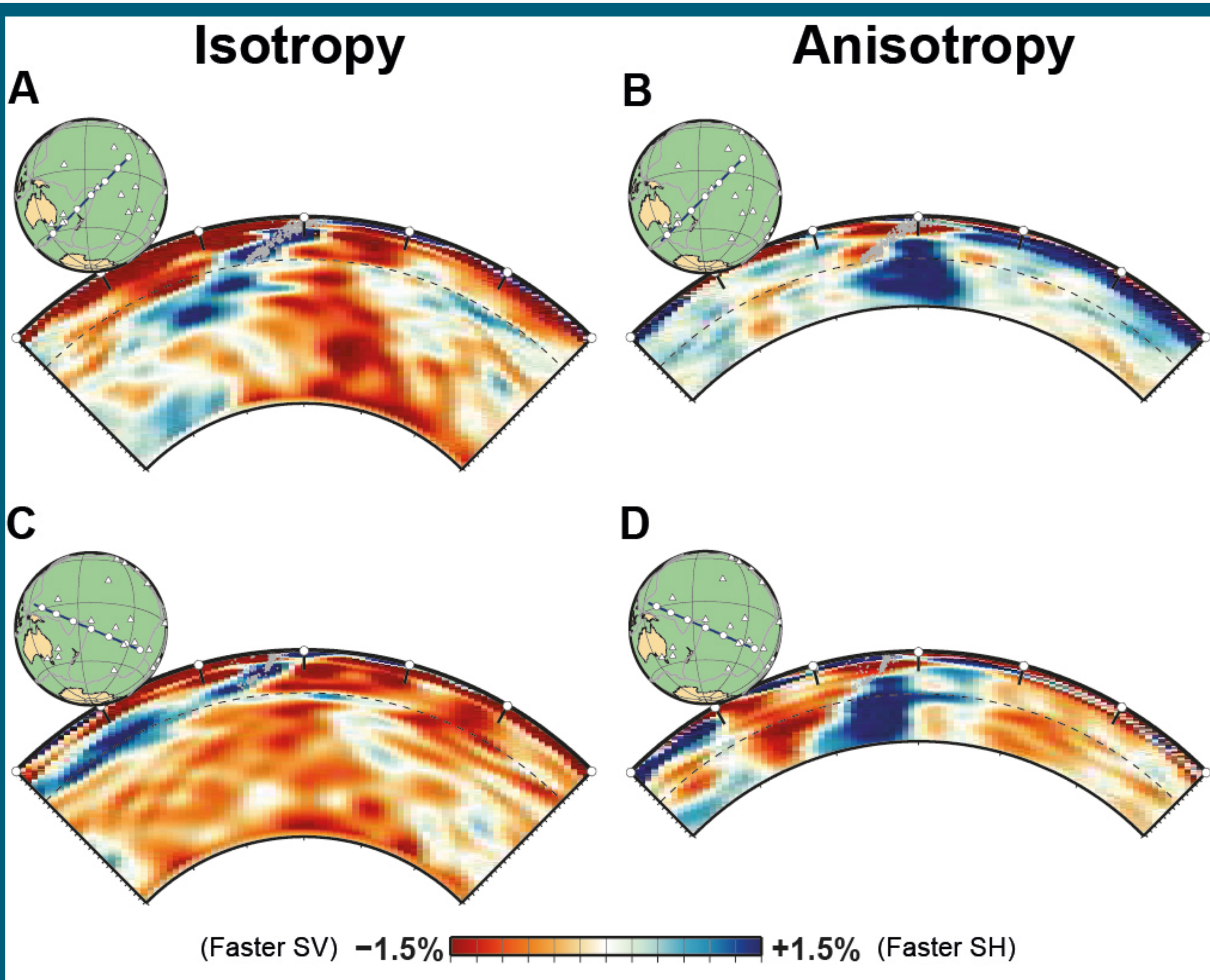
Isotropy
Anisotropy
A
B
C
D
(Faster SV) −1.5%
+1.5% (Faster SH)

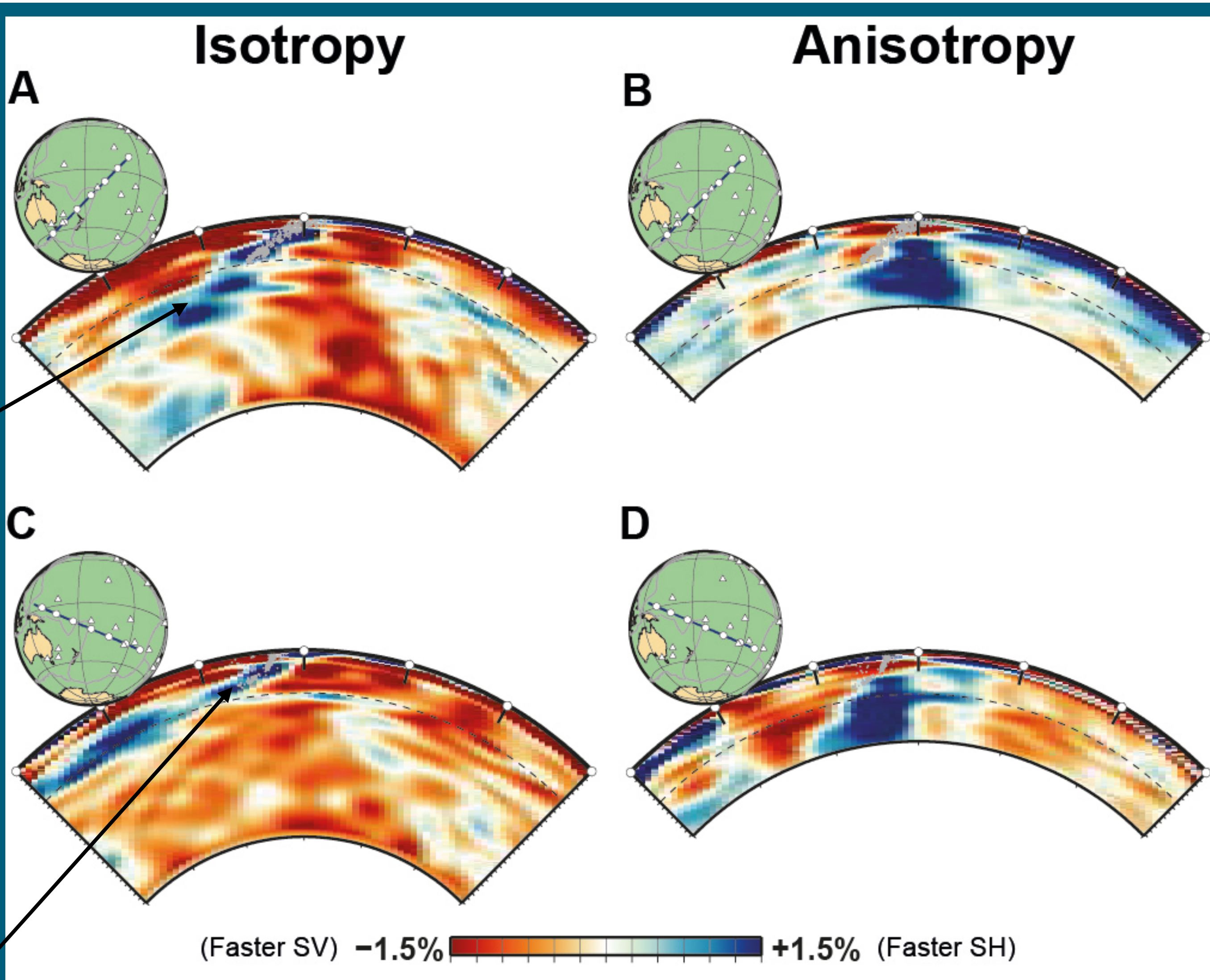

Kermadec: down to LM

Tonga slab: stagnant in the TZ

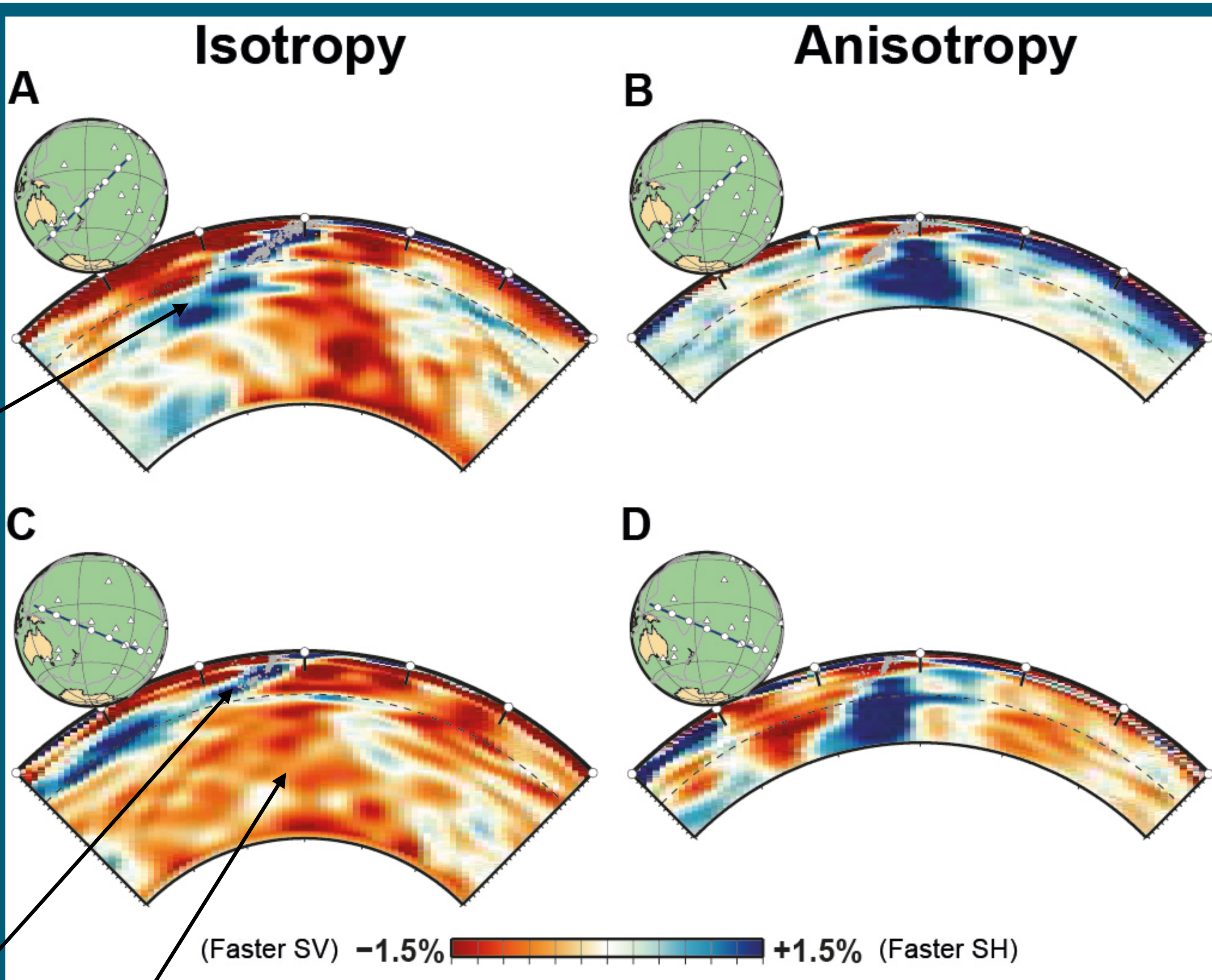

Kermadec: down to LM

Tonga slab: stagnant in the TZ

Large scale upwelling (Samoan plume) from mega-ULVZ in Pacific LLSVP

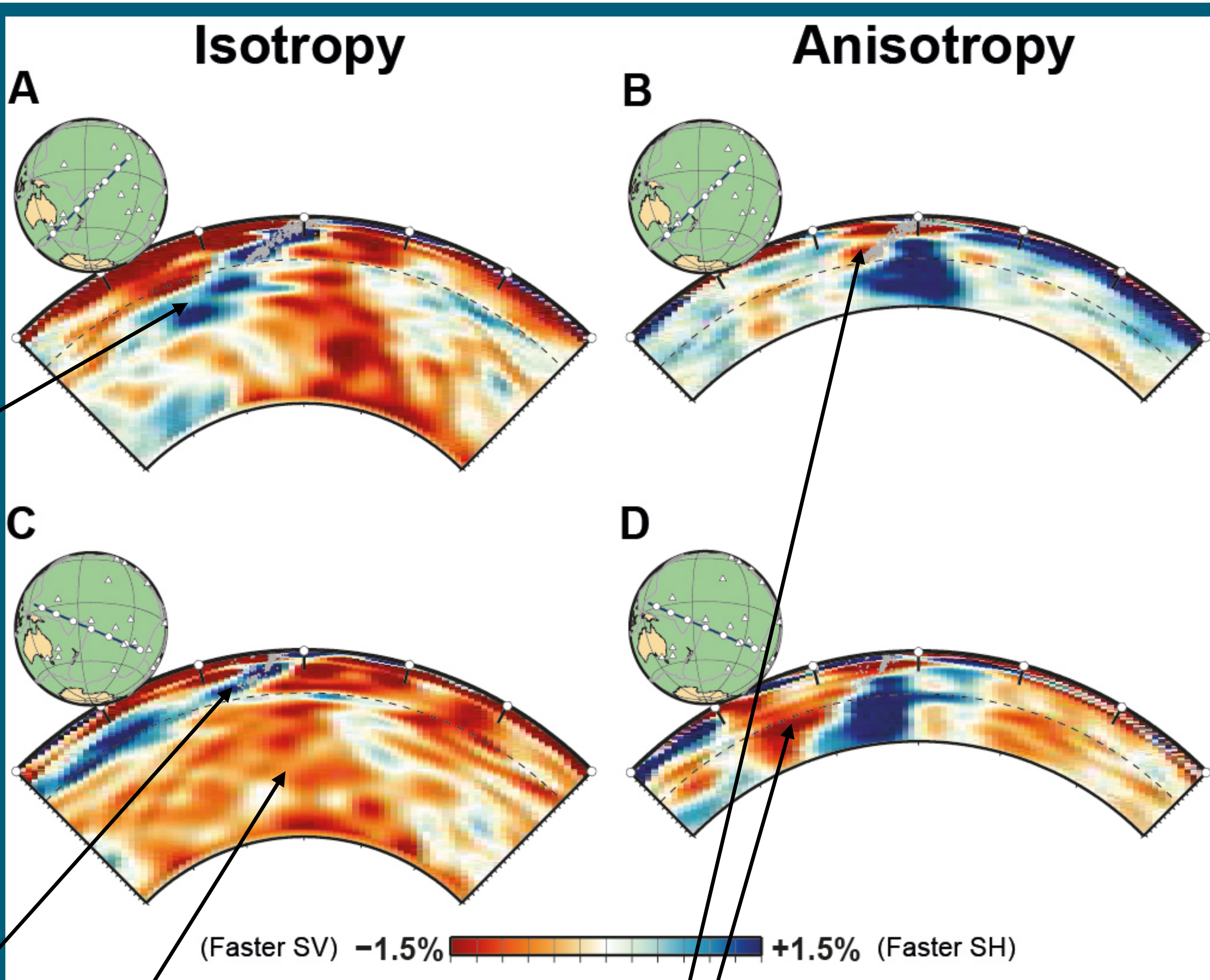

Kermadec: down to LM

Tonga slab: stagnant in the TZ

Large scale upwelling (Samoan plume) from mega-ULVZ in Pacific LLSVP

Faster SV anomalies associated with slabs

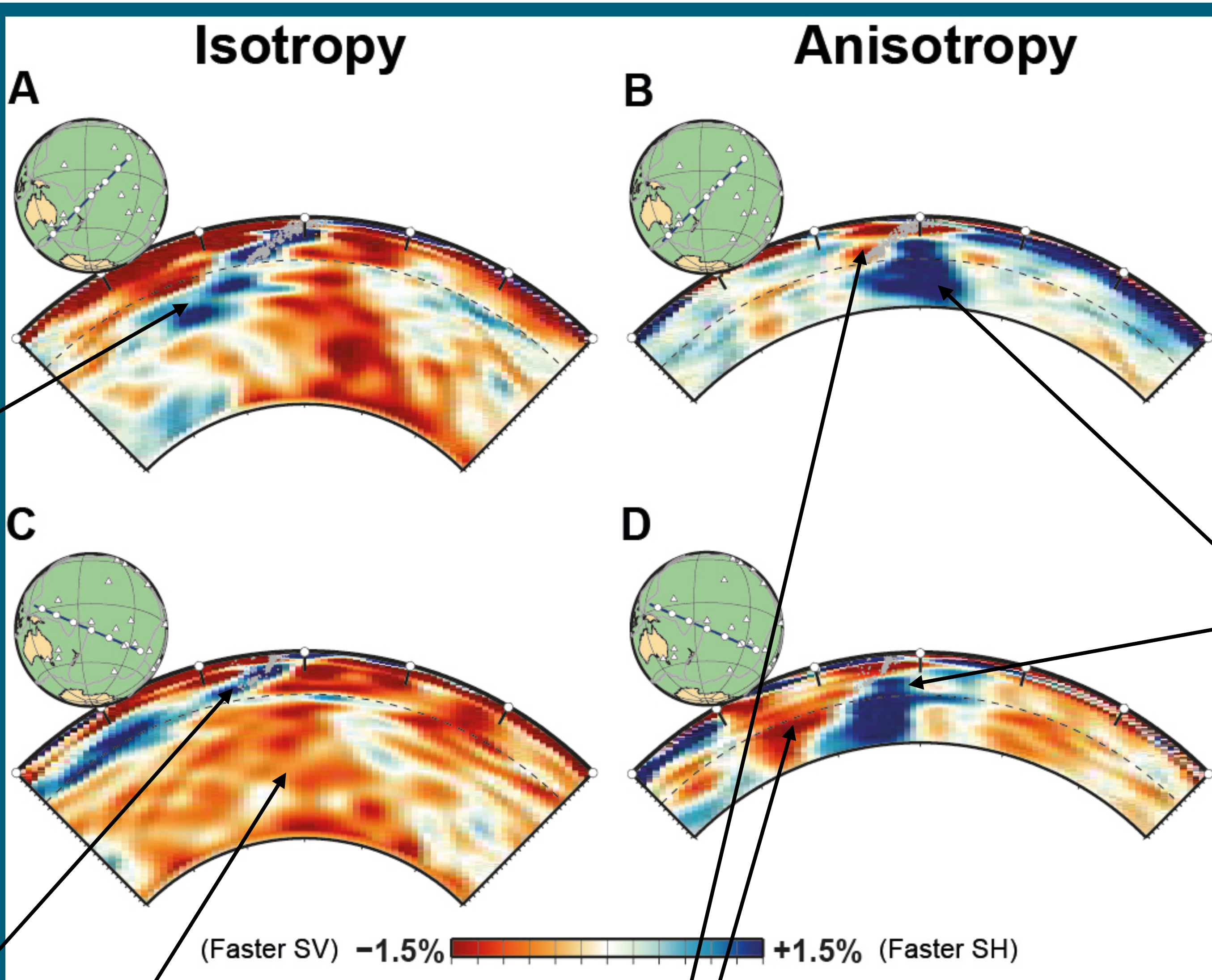

Kermadec: down to LM

~1000 km faster SH anomaly behind slab following the upwelling

Tonga slab: stagnant in the TZ

Large scale upwelling (Samoan plume) from mega-ULVZ in Pacific LLSVP

Faster SV anomalies associated with slabs

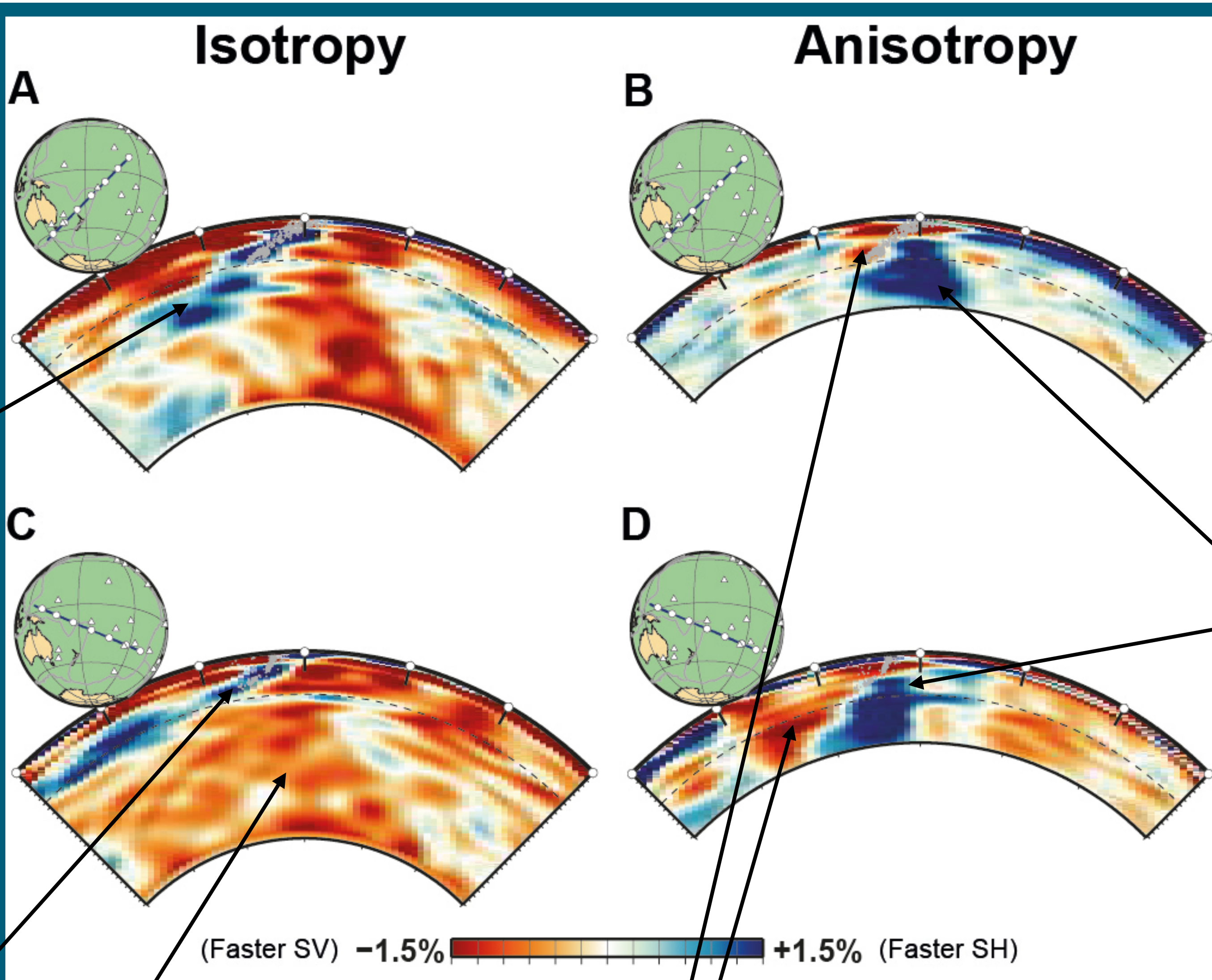

Kermadec: down to LM

Tonga slab: stagnant in the TZ

~1000 km faster SH anomaly behind slab following the upwelling

Large scale upwelling (Samoan plume) from mega-ULVZ in Pacific LLSVP

Faster SV anomalies associated with slabs

Strong, deep plume-slab interaction:
-plume plays an active role?
-contributes to fast slab retreat and basin opening?

Chang, Ferreira and Faccenda, Nature Comms., 2016

3-D geodynamic modelling

(Faccenda, PEPI, 2014):

- 3D petrological-thermo-mechanical modelling: Composite visco-plastic rheology; effective viscosity combines dislocation and diffusion creep mechanisms; includes phase transitions for a pyrolitic mantle composition.

- Mantle fabric modelling: Compute LPO of mantle polycrystalline aggregates (D-Rex modified to account for non-steady-state deformation and deformation history in the mid-mantle). Use reported slip systems of olivine, enstatite and wadsleyite. For bridgmanite test slip systems from experimental studies and ab-initio models.

- Obtain elastic properties of the aggregates by Voigt-averaging the crystal elastic properties scaled by local P-T conditions (e.g., Vp, Vs and radial anisotropy)

- Test different scenarios, e.g.:

with and without plume; with and without Hikurangi plateau; ten different slip systems of bridgmanite

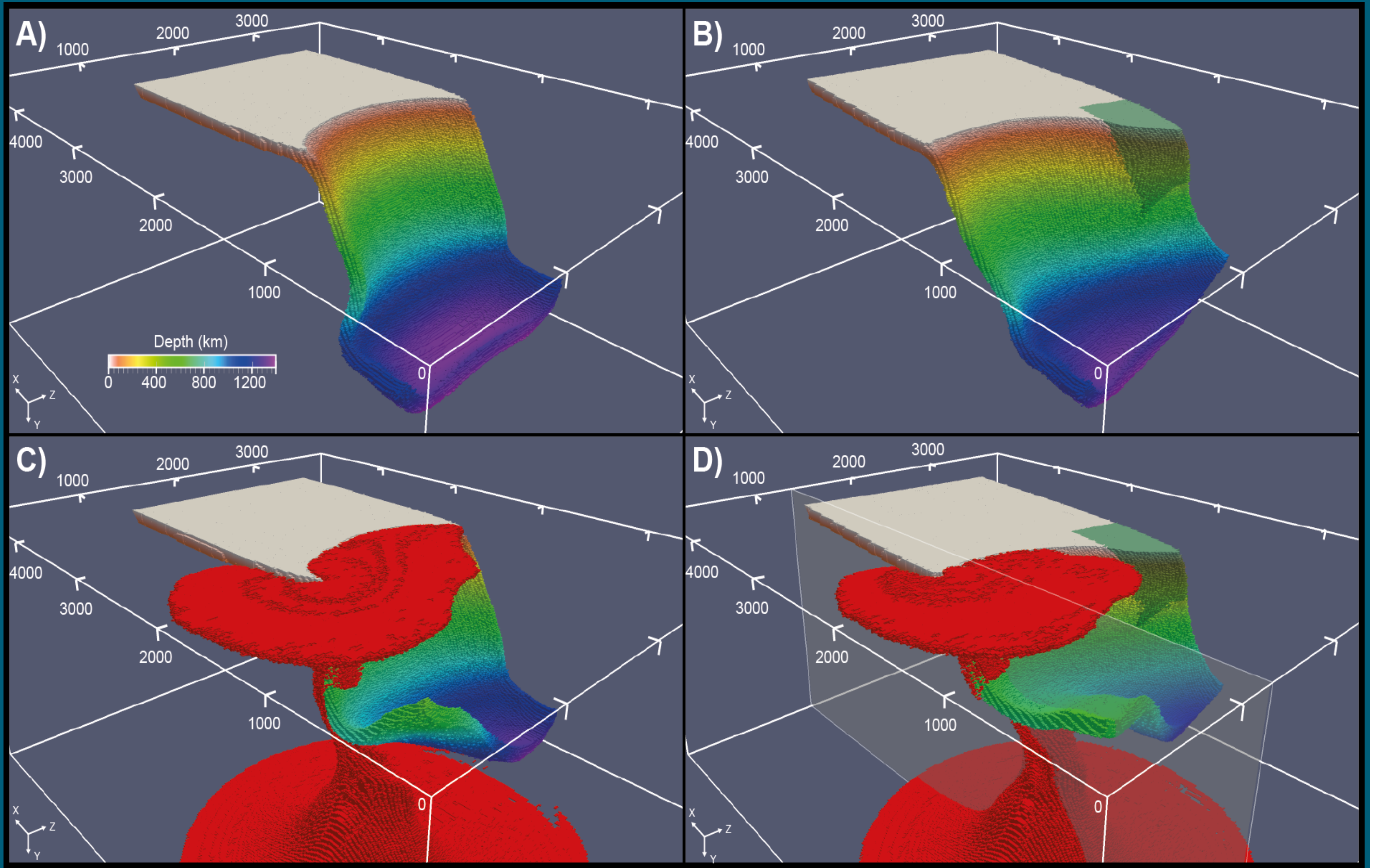

Chang, Ferreira and Faccenda, Nature Comms., 2016

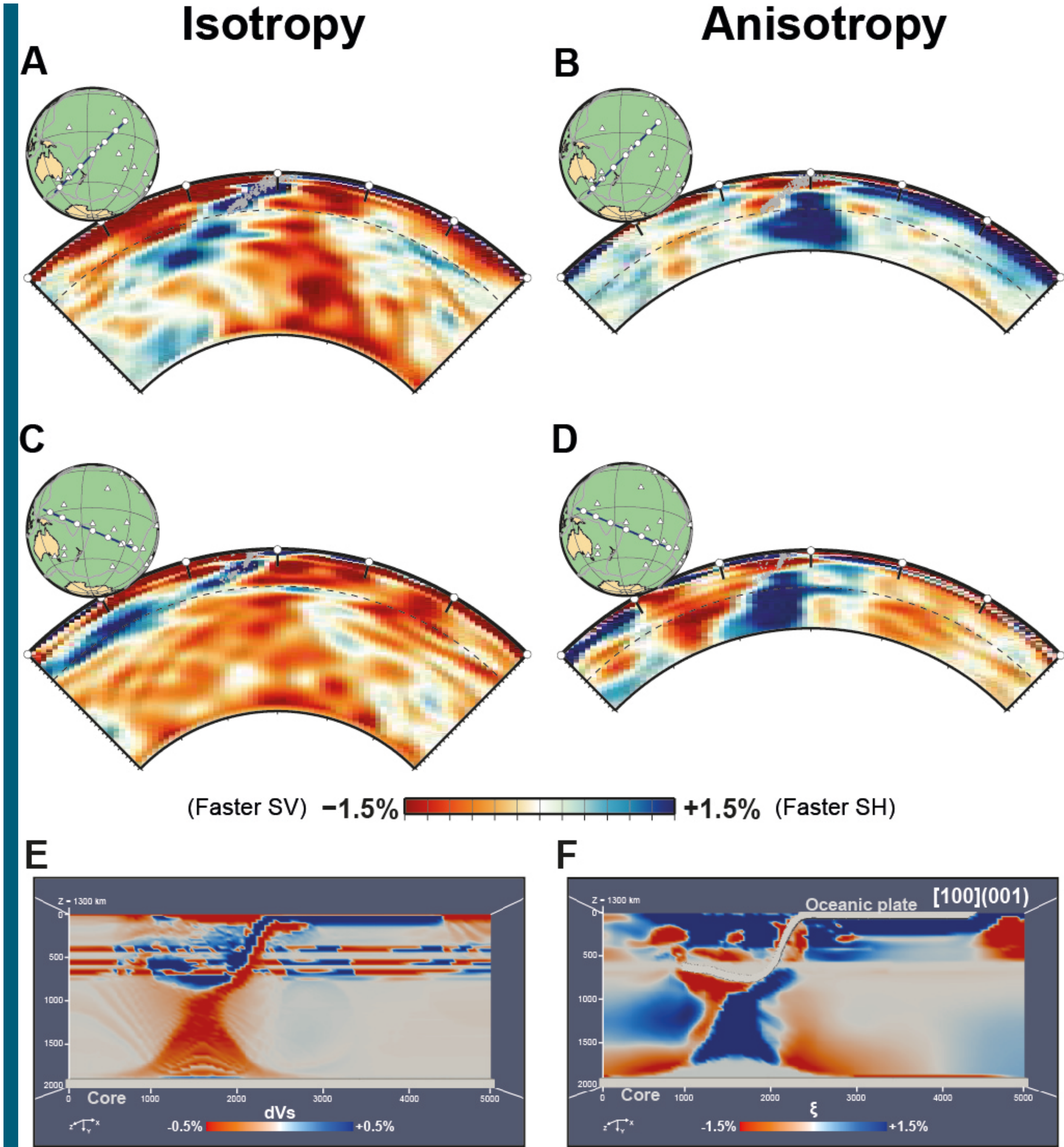

- The upwelling plume favors slab stagnancy in the TZ
- The entrainment of the Hikurangi plateau promotes fast trench retreat on the Tonga slab
- In turn, the fast trench rollback increases the subduction velocity and the tendency of the slab to stagnate in the TZ: coupled plume-fast slab retreat effect
- Identified possible dominant slip systems of bridgmanite

Conclusions

- Inaccurate crustal corrections have a strong influence on anisotropy imaging. We invert for crustal thickness perturbations to reduce the crustal effects on mantle structure imaging.
- Our global isotropic model shows small-scale features observed in other upper-mantle models and well delineated subduction slabs.
- It is difficult to constrain D'' anisotropy globally.
- The upper mantle structure in our anisotropic model is consistent with other studies, notably with high-resolution regional studies.
- We observe faster SV velocity anomalies along subduction zones beneath the Western Pacific in the transition zone and faster SH in the uppermost lower mantle.
- A strong, ~1000 km, robust faster SH anomaly is observed beneath Tonga down to ~1400 km possibly indicating deep plume-slab interaction with the upwelling playing a very active role, which is consistent with results from geodynamical modelling.